International Journal of
Molecular Microbiology

Research Article 2025 | Volume 8 | Issue 1 | 52-69

Open Access

Article Information

Received: October 10, 2025

Accepted: October 30, 2025

Published: November 7, 2025

Keywords

Apoptozole,
Cystic fibrosis,
Drug discovery,
Molecular docking,
Structural modeling.

Authors' Contribution

AN and AW conceived and designed the study; KR, NS, and AI performed the experiments and analyzed the results; ZA, HUT, and MP wrote and revised the manuscript.

How to cite

Noman, A., Sardar, N., Islam, A., Ramzan, K., Ali, M.Z., Tahir, H.U., Waheed, A., Parveen, M., 2025. Integrative Computational Analysis of CFTR Mutations Linked to Cystic Fibrosis. Int. J. Mol. Microbiol., 8(1): 52-69.

***Correspondence**

Ali Noman
Email: alinoman1907@gmail.com

Integrative Computational Analysis of CFTR Mutations Linked to Cystic Fibrosis

Ali Noman[1*], Nimra Sardar[2], Amina Islam[2], Kainat Ramzan[3], Muhammad Zeeshan Ali[2], Habib Ullah Tahir[2], Ayesha Waheed[3], Maria Parveen[4]

[1]Department of Zoology, University of Okara, Okara, Pakistan.
[2]Department of Microbiology and Molecular Genetics, University of Okara, Okara, Pakistan.
[3]Department of Biochemistry, University of Okara, Renala Khurd, Okara, Pakistan.
[4]Department of Molecular Biology, University of Okara, Okara, Pakistan.

Abstract:

The CFTR gene encodes a chloride channel essential for epithelial ion transport, and deleterious nsSNPs are a major cause of cystic fibrosis (CF). CF is an autosomal recessive disorder affecting multiple systems, with symptoms including chronic cough, recurrent lung infections, bronchiectasis, reduced pulmonary function, pancreatic insufficiency, malabsorption, poor growth, salty-tasting skin, male infertility, liver disease, and diabetes. To date, over 4,000 CFTR mutations have been reported, with F508del being the most common, accounting for nearly 70% of cases. This study aimed to identify deleterious nsSNPs in the CFTR gene and evaluate their structural and functional impact using an integrative in silico pipeline. Additionally, molecular docking was performed to explore potential therapeutic modulators for cystic fibrosis. The NCBI database reported over 282,000 SNPs in CFTR, of which SNPnexus analysis identified 132 nsSNPs as highly deleterious. Furthermore, 30 nsSNPs were consistently predicted to be deleterious across 15 computational tools. Notably, variants such as I105N, K273Q, and G1249R demonstrated destabilizing effects, with RMSD values ranging from 0.93 to 0.98 Å, indicating substantial conformational alterations. Molecular docking revealed strong ligand interactions with both wild-type and mutant CFTR, particularly for apoptozole, Congo Red, NAD, melanin, and cAMP, while repurposed drugs such as nelfinavir and amprenavir demonstrated favorable binding, supporting their potential to rescue misfolded proteins. This integrative in silico study highlights 30 pathogenic CFTR nsSNPs with destabilizing structural effects and identifies potential modulators, providing a robust framework for experimental validation, drug repurposing, and personalized therapeutic strategies in cystic fibrosis.

Scan QR code to visit this journal.

INTRODUCTION

Cystic fibrosis (CF) is an autosomal recessive disorder caused by mutations in the cystic fibrosis transmembrane conductance regulator (CFTR) gene, with over 4000 variants identified (Ideozu *et al.*, 2024b; Rafique *et al.*, 2024). The CFTR protein functions as a chloride channel, regulating ion balance to maintain thin mucus and proper epithelial hydration. CF leads to thick mucus, causing chronic lung infections, pancreatic insufficiency, malabsorption, poor growth, and infertility (Purushothaman and Nelson, 2023). CFTR mutations are grouped into six classes (I–VI) based on their effects on protein production, folding, trafficking, and stability. Missense mutations are most common. Classes I–III abolish function, causing severe disease, while Classes IV–VI retain partial activity with milder symptoms. Notable mutations include G542X (Class I), F508del (Class II), and G551D (Class III) (Deletang and Taulan-Cadars, 2022; Ramananda *et al.*, 2024). Additionally, polymorphism in CFTR coding and regulatory regions affect its expression and function, contributing to clinical variability (Parisi *et al.*, 2022; Zhu, 2024).

The CFTR gene, mapped on chromosome 7q31.2 (NC_000007.14), spans about 190 kb and contains 27 exons encoding a 6.5 kb mRNA that translates into a 1,480–amino acid protein. After folding and glycosylation in the endoplasmic reticulum, it traffics through the Golgi to the apical membrane, where it mediates chloride and bicarbonate transport. Structurally, CFTR belongs to the ATP-binding cassette (ABC) transporter family and is composed of two membrane-spanning domains (MSD1 and MSD2) that form the channel, two nucleotide-binding domains (NBD1 and NBD2) that regulate ATP-driven gating, and a regulatory (R) domain that controls channel activity. Moreover, CFTR also transports glutathione, contributing to epithelial homeostasis (Ideozu *et al.*, 2024b; Zhang *et al.*, 2025).

Over 1,900 CFTR variants have been described, with ~1,500 linked to disease (Mathew *et al.*, 2021). The ΔF508 variant, present in over 70% of cases, disrupts CFTR folding and trafficking, impairing chloride transport. This causes thick secretions that affect the respiratory, digestive, and reproductive systems, with lung complications being the leading cause of morbidity and mortality (Doss *et al.*, 2008). Moreover, CFTR is a phosphorylation-regulated by protein kinase A or C, enabling ATP binding and channel opening, allowing chloride flow with sodium and water. Disruption impairs mucociliary clearance and fluid balance, leading to complications such as diarrhea or constipation. Moreover, missense mutations in CFTR can disrupt transcription factor binding, regulatory elements, or splicing enhancers, thereby altering gene expression. This study employed an in-silico approach to assess the impact of nsSNPs on CFTR structure and function. Homology modeling and virtual screening were used to explore ligand interactions, revealing variant-induced destabilization. These findings advance understanding of cystic fibrosis pathogenesis and support future therapeutic development.

MATERIALS AND METHODS

Mining datasets

The CFTR protein sequence was obtained from UniProtKB (https://www.uniprot.org) and the NCBI database (http://www.ncbi.nlm.nih.gov). For computational analysis, the complete SNP dataset of the human CFTR gene was retrieved from dbSNP-NCBI (https://www.ncbi.nlm.nih.gov/snp), and the overall methodology is presented in Figure (1).

Bioinformatics Tools for nsSNP Analysis

Several bioinformatics tools were employed to analyze nsSNPs obtained from the dbSNP database. SNPnexus (https://www.snp-nexus.org) integrates multiple prediction algorithms, including SIFT and PolyPhen. SNAP2 (https://rostlab.org/services/snap2web) evaluates the functional impact of polymorphisms using the FASTA sequence as input, enabling genome-wide comparisons. PROVEAN (http://provean.jcvi.org/index.php) applies alignment-based scoring, with variants

scoring below - 2.5 considered deleterious. PolyPhen-2 (http://genetics.bwh.harvard.edu/pph2) predicts substitution effects on a scale from 0 (benign) to 1 (damaging). CADD (https://cadd.gs.washington.edu) provides integrative annotations for genome variants, including point mutations and indels. CONDEL (https://bbglab.irbbarcelona.org/fannsdb) classifies nsSNPs as either neutral (0) or deleterious (1) (Tariq *et al.*, 2024a; Waheed *et al.*, 2024).

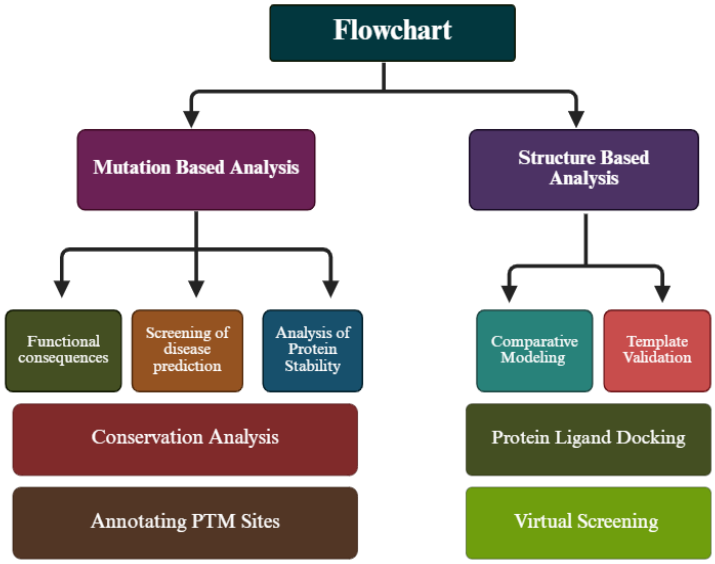

Fig. 1. Schematic representation of the CFTR gene workflow used in this study.

The SNPs & GO tool (https://snps-and-go.biocomp.unibo.it/snps-and-go) evaluates amino acid substitutions at specific protein sites using Uniprot ID and mutation position as input. Meta-SNP (https://snps.biofold.org/meta-snp) predicts SNVs with an accuracy of ~79%; scores >0.5 are considered damaging (AbdulAzeez and Borgio, 2016; Hasnain *et al.*, 2020; Magesh and Doss, 2014; Subbiah *et al.*, 2020). P-MUT (http://mmb.irbbarcelona.org/PMut) predicts the pathological impact of mutations with ~80% accuracy and provides access to all single amino acid variants for disease association analysis (López-Ferrando *et al.*, 2017). PhD-SNP (https://snps.biofold.org/phd-snp.html) achieves ~78% accuracy and uses a 0–9 scoring scale to assess disease-related mutations (Abuzaid *et al.*, 2024).

Prediction of Protein Stability Alterations

The stability effects of CFTR mutations were assessed by predicting changes in free energy. MUpro (http://mupro.proteomics.ics.uci.edu) estimates ΔΔG values, where scores ≤0 indicate decreased protein stability. I-Mutant 3.0 (http://gpcr2.biocomp.unibo.it/cgi/predictors/I-Mutant3.0/I-Mutant3.0.cgi) predicts stability alterations with ~77% accuracy (Kamal *et al.*, 2025; Sharma *et al.*, 2024). i-Stable (http://predictor.nchu.edu.tw/istable) uses support vector machine (SVM) algorithms to evaluate the impact of amino acid substitutions on protein stability (Waheed *et al.*, 2024).

Conservation analysis and PTM sites

Evolutionary conservation of CFTR amino acid residues was assessed using ConSurf (https://consurf.tau.ac.il). Conservation scores ranged from 1 to 9, with values 1–3 indicating

variable regions, 4–6 moderate conservation, and 7–9 highly conserved sites (Armon *et al.*, 2001; Hasnain *et al.*, 2020; Subbiah *et al.*, 2020)**.** PTM analysis was conducted to evaluate the potential effects of CFTR variants on protein regulation through modifications such as phosphorylation, acetylation, methylation, and ubiquitination (Hasan and Khatun, 2018). Phosphorylation sites in the CFTR protein were predicted using MusiteDeep (https://www.musite.net), with the amino acid sequence provided as input (Chandrasekaran *et al.*, 2017; Wang *et al.*, 2020).

Structural Modeling and Validation

The CFTR protein structure was modeled using SWISS-MODEL (https://swissmodel.expasy.org), and specific mutations were introduced using PyMOL (http://www.pymol.org) (Bilal *et al.*, 2025a; Bilal *et al.*, 2025b). The models were refined with ModRefiner (https://zhanggroup.org/ModRefiner) to optimize geometry and stereochemistry. Model quality was assessed via the SAVES server (https://saves.mbi.ucla.edu), which integrates PROCHECK, ERRAT, and Verify3D (Heidarinia *et al.*, 2025). The Ramachandran plot is generated using the Ramplot server (https://www.ramplot.in/index.php) evaluates backbone torsion angles (φ, ψ) to ensure proper stereochemistry (Kumar and Rathore, 2025). Finally, the overall reliability of the predicted structure was verified using QMEAN **(**https://swissmodel.expasy.org/qmean**)**, which calculates a composite score based on local geometry, long-range interactions, and solvation energy; a Z-score near zero indicates high structural quality (Ramzan and Noman, 2024). Moreover, Structural deviations between wild-type and mutant models were compared using TM-align (https://zhanggroup.org/TM-align), with RMSD values used to quantify conformational differences. The structural effects of amino acid substitutions were analyzed using the HOPE server (https://www3.cmbi.umcn.nl/hope), which evaluates changes in size, charge, and hydrophobicity, considering conserved regions and functional domains to predict impacts on protein stability and function (Kumari *et al.*, 2025; Rasheed *et al.*, 2025).

Virtual Screening and Molecular Docking

Virtual screening was conducted to identify potential ligands interacting with CFTR variants. Ligand structures were retrieved from PubChem (https://pubchem.ncbi.nlm.nih.gov) and relevant literature. Docking simulations were performed using PyRx (https://pyrx.sourceforge.io), which utilizes AutoDock Vina for protein–ligand docking. Protein and ligand structures were converted to PDBQT format before docking. The interactions of the resulting docked complexes were visualized and analyzed in both 2D and 3D using Discovery Studio Visualizer (https://discover.3ds.com/discovery-studio-visualizer-download) (Adeniji *et al.*, 2020; Ramzan and Noman, 2024; Tariq *et al.*, 2024b).

RESULTS

Retrieval of Functional SNPs

A total of 282,490 SNPs in the human CFTR gene were retrieved from NCBI dbSNP and analyzed using SNPnexus. Of these, 10,618 were non-synonymous, 233,126 were in coding regions, 32,781 were in the non-coding areas, 2,327 were in untranslated regions, 7,671 were in the 5′ upstream, 6,585 were in the 3′ downstream, and 2,049 were synonymous. Their distribution across the CFTR gene is shown in Figure (2A). This study emphasizes coding-region variants, with non-synonymous SNPs accounting for only a small fraction. For further analysis, we focused on non-synonymous SNPs because they can alter amino acid sequences and affect CFTR protein structure and function. The SIFT algorithm predicted 5,124 SNPs as deleterious and 3,474 as tolerated. PolyPhen identified 4,367 SNPs as potentially damaging (Figure 2B). Notably, 132 variants were consistently predicted as deleterious by both SIFT (score = 0.00) and PolyPhen (score = 1.00), indicating high deleterious variants (Table 1).

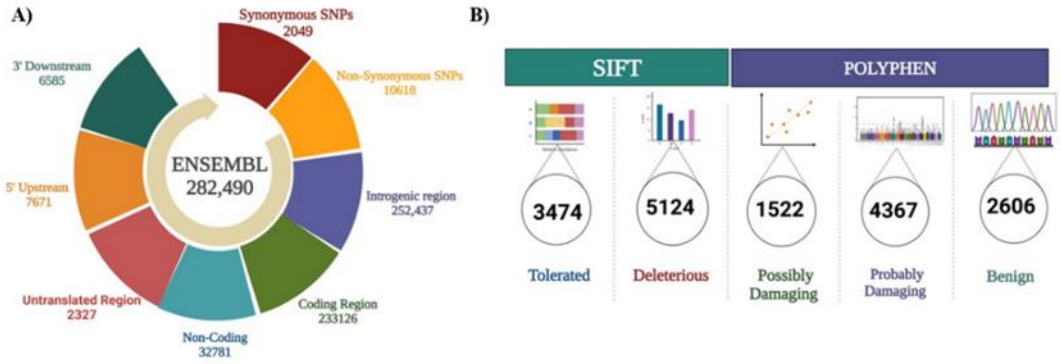

Fig. 2. A) Donut chart showing the distribution of SNPs across the CFTR gene regions **B)** SIFT and PolyPhen algorithm outcomes.

Table 1. SNPnexus predictions of highly deleterious and probably damaging CFTR gene variants.

		SIFT		PolyPhen				SIFT		PolyPhen				SIFT		PolyPhen	
Variation ID	**Protein Change**	Score	Effect	Score	Effect	Variation ID	Protein Change	Score	Effect	Score	Effect	Variation ID	Protein Change	Score	Effect	Score	Effect
rs1031657153	P99A	0	D	1	Prob Damage	rs377514639	R258I	0	D	1	Prob Damage	rs1299482973	S707F	0	D	1	Prob Damage
rs397508467	P99L	0	D	1	Prob Damage	rs1296578005	K273Q	0	D	1	Prob Damage	rs397508375	D806G	0	D	1	Prob Damage
rs397508490	L102P	0	D	1	Prob Damage	rs756036343	K273M	0	D	1	Prob Damage	rs757165481	Y849H	0	D	1	Prob Damage
rs397508509	I105N	0	D	1	Prob Damage	rs397508800	W277R	0	D	1	Prob Damage	rs775570582	L165S	0	D	1	Prob Damage
rs397508522	Y109N	0	D	1	Prob Damage	rs151073129	I285F	0	D	1	Prob Damage	rs1402844924	L165F	0	D	1	Prob Damage
rs121909031	Y109C	0	D	1	Prob Damage	rs1204521684	V317G	0	D	1	Prob Damage	rs121909035	H949Y	0	D	1	Prob Damage
rs113993958	D110Y	0	D	1	Prob Damage	rs121909011	R334W	0	D	1	Prob Damage	rs397508444	H949R	0	D	1	Prob Damage
rs140502196	P111L	0	D	1	Prob Damage	rs397508146	L346P	0	D	1	Prob Damage	rs1191342069	G1241D	0	D	1	Prob Damage
rs397508551	N113I	0	D	1	Prob Damage	rs77932196	R347P	0	D	1	Prob Damage	rs397508599	G1244R	0	D	1	Prob Damage
rs761370893	E116G	0	D	1	Prob Damage	rs397508188	L441P	0	D	1	Prob Damage	rs267606723	G1244E	0	D	1	Prob Damage
rs201958172	A120P	0	D	1	Prob Damage	rs121908805	S466L	0	D	1	Prob Damage	rs397508602	G1249R	0	D	1	Prob Damage
rs397508592	Y122H	0	D	1	Prob Damage	rs1800089	L467F	0	D	1	Prob Damage	rs121909040	G1249E	0	D	1	Prob Damage
rs377295859	Y122C	0	D	1	Prob Damage	rs139573311	L467P	0	D	1	Prob Damage	rs117400534	L1253F	0	D	1	Prob Damage
rs397508609	G126D	0	D	1	Prob Damage	rs397508202	L468P	0	D	1	Prob Damage	rs11971167	D1270Y	0	D	1	Prob Damage
rs1162745955	L129H	0	D	1	Prob Damage	rs79282516	G480S	0	D	1	Prob Damage	rs765549490	D1270G	0	D	1	Prob Damage
rs397508674	L137H	0	D	1	Prob Damage	rs397508208	G480D	0	D	1	Prob Damage	rs753920616	F508V	0	D	1	Prob Damage
rs1800078	L138P	0	D	1	Prob Damage	rs200626971	W496C	0	D	1	Prob Damage	rs77010898	W1282 C	0	D	1	Prob Damage
rs397508718	G149R	0	D	1	Prob Damage	rs774945680	G500D	0	D	1	Prob Damage	rs77902683	R1283M	0	D	1	Prob Damage
rs397508719	G149E	0	D	1	Prob Damage	rs397508222	I502N	0	D	1	Prob Damage	rs904990724	G1298R	0	D	1	Prob Damage
rs397508723	A155P	0	D	1	Prob Damage	rs397508224	I506S	0	D	1	Prob Damage	rs193922522	G1298A	0	D	1	Prob Damage
rs397508724	S158C	0	D	1	Prob Damage	rs1800092	I506M	0	D	1	Prob Damage	rs121909042	N1303H	0	D	1	Prob Damage

rs397508727	L159S	0	D	1	Prob Damage	rs74571530	F508C	0	D	1	Prob Damage	rs121909042	N1303Y	0	D	1	Prob Damage
rs397508729	Y161D	0	D	1	Prob Damage	rs758745885	D513Y	0	D	1	Prob Damage	rs397508636	N1303I	0	D	1	Prob Damage
rs397508730	Y161S	0	D	1	Prob Damage	rs368516826	C524R	0	D	1	Prob Damage	rs80034486	N1303K	0	D	1	Prob Damage
rs397508736	L165S	0	D	1	Prob Damage	rs1387755887	G545V	0	D	1	Prob Damage	rs201503139	P1306S	0	D	1	Prob Damage
rs80282562	G178R	0	D	1	Prob Damage	rs1469024267	L548P	0	D	1	Prob Damage	rs397508646	D1312G	0	D	1	Prob Damage

* D: Deleterious; Prob Damage: Probably Damaging

Annotation of missense SNPs

The analysis of 132 high-confidence CFTR nsSNPs revealed distinct patterns of deleterious and neutral variants across multiple prediction tools (Supplementary Table S1). SNAP2 identified 115 variants as functionally deleterious, while P111L, N113I, S519R, S519I, G551D, R555G, V562I, L564P, F587L, Q590R, D614N, T652A, R668H, S737F, Q768H, L1335F, and I1366M were predicted neutral. PROVEAN classified 112 nsSNPs as deleterious and 20 as neutral, including the same variants plus P574H, L1369F, and D1370H. CADD scores highlighted high pathogenic potential for K273Q (41), L165S (41), G1244R (43), L1356S (44), G149R (38), W1282C (46), G1298R (48), and R560G (49), whereas neutral variants scored below 40. ConDEL predictions indicated neutrality for S519I (0.541), S519R (0.462), G551D (0.752), and R555G (0.799). PolyPhen-2 classified all 132 nsSNPs as probably damaging (Figure 3). Collectively, these analyses suggest that these nsSNPs are likely to significantly impact CFTR structure and function.

In Figure (3), analysis of 132 CFTR nsSNPs revealed that all variants were predicted to be disease-causing by SNP & GO. P-Mut classified most variants as disease-related but identified six variants as neutral, including E116G (0.4718), D192G (0.4395), L467F (0.4722), S519R (0.4215), Q767H (0.4504), and S707F (0.4427). PhD-SNP predicted 40 nsSNPs as neutral, including P111L, N113I, E116G, A120P, Y122H, Y122C, S158C, L159S, L165S, L183I, D192N, D192G, L180F, W216C, G241W, I1267M, L1339F, A1364V, I1366M, H949Y, H949R, G1298A, and P1306S, while the remaining 92 variants were classified as disease-causing. Meta-SNP predicted 12 neutral variants, including P111L, N113I, E116G, S519I, S519R, S707F, I1267M, L1369F, H949Y, Q767H, G1298A, and D1370H, confirming that the majority of nsSNPs are likely pathogenic (Supplementary Table S2).

Variant Effect on Protein Stability

In Figure (3), a total of 132 nsSNPs were submitted to i-Mutant 3.0 for RI prediction, revealing that 21 nsSNPs increase protein stability, including P99L, K273M, L441P, G545V, S707F, G178E, N113I, A120P, G226E, S519R, S519I, G1249E, G1249R, I1366I, and so on. Additionally, MUPro analysis indicated that P99L, K273M, L441P, G545V, and S707F enhance CFTR stability. As summarized in Table (S3), i-Stable predicted that 26 nsSNPs increase protein stability, whereas 106 missense variants lead to decreased stability, highlighting the overall destabilizing impact of most CFTR mutations.

Evolutionary Conservation and PTM Analysis

A total of 132 nsSNPs in the CFTR gene were examined to evaluate their evolutionary conservation and possible post-translational modifications (PTMs). Analysis with CONSURF showed that most variants are located in highly conserved regions, with scores ranging from 1 to 9 (Table 2). Of these, 98 nsSNPs had scores between 7 and 9, suggesting important roles in protein structure or function, and 46 variants scored the maximum of 9, indicating residues that are highly conserved and likely critical for protein activity. PTM analysis using Musite Deep predicted three sites of potential modification such as C524 as an S-palmitoyl cysteine, and S707 and S737 as phosphoserine residues. These sites may play regulatory roles affecting the stability and function of the CFTR protein. Combining the information from conservation

and PTM analyses allows identification of nsSNPs with the highest potential to disrupt protein function, which can be prioritized for further structural and functional studies.

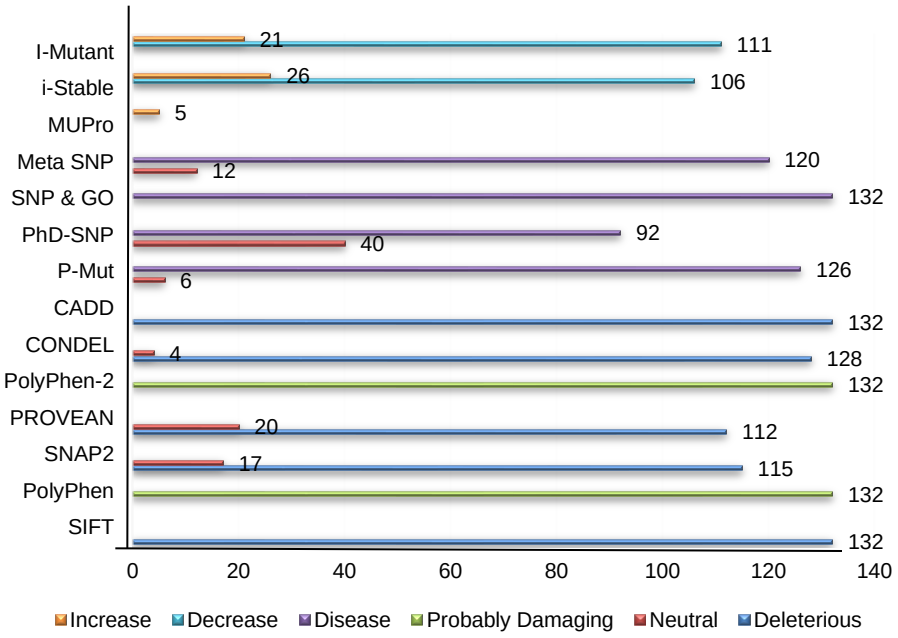

Fig. 3. In silico prediction of CFTR nsSNP functional and stability analysis.

Table 2. Identification of Evolutionary Conservation of nsSNPs in the CFTR Gene.

Variation ID	Mutation	ConSURF Score	Variation ID	Mutation	ConSURF Score	Variation ID	Mutation	ConSURF Score
rs1031657153	P99A	9,e,f	rs377514639	R258I	9,e,f	rs1299482973	S707F	7,e
rs397508467	P99L	9,e,f	rs1296578005	K273Q	9,e,f	rs397508375	D806G	9,b,s
rs397508490	L102P	8,b	rs756036343	K273M	9,e,f	rs757165481	Y849H	9,e,f
rs397508509	I105N	9,b,s	rs397508800	W277R	9,b,s	rs775570582	L165S	8,b
rs397508522	Y109N	7,b	rs151073129	I285F	8,b	rs1402844924	L165F	8,b
rs121909031	Y109C	7,b	rs1204521684	V317G	6,b	rs121909035	H949Y	5,e
rs113993958	D110Y	5,e	rs121909011	R334W	7,e	rs397508444	H949R	5,e
rs140502196	P111L	1,e	rs397508146	L346P	6,b	rs1191342069	G1241D	8,b
rs397508551	N113I	4,e	rs77932196	R347P	9,e,f	rs397508599	G1244R	9,b,s
rs761370893	E116G	6,e	rs397508188	L441P	9,e,f	rs267606723	G1244E	9,b,s
rs201958172	A120P	7,b	rs121908805	S466L	8,b	rs397508602	G1249R	9,e,f
rs397508592	Y122H	1,b	rs1800089	L467F	8,b	rs121909040	G1249E	9,e,f
rs377295859	Y122C	1,b	rs139573311	L467P	8,b	rs117400534	L1253F	7,b
rs397508609	G126D	7,b	rs397508202	L468P	6,b	rs11971167	D1270Y	8,e,f
rs1162745955	L129H	4,b	rs79282516	G480S	8,e,f	rs765549490	D1270G	8,e,f
rs397508674	L137H	4,b	rs397508208	G480D	8,e,f	rs753920616	F508V	7,b
rs1800078	L138P	4,b	rs200626971	W496C	6,b	rs77010898	W1282C	8,b
rs397508718	G149R	8,b	rs774945680	G500D	3,b	rs77902683	R1283M	9,e,f
rs397508719	G149E	8,b	rs397508222	I502N	7,b	rs904990724	G1298R	5,b

rs397508723	A155P	9,b,s	rs397508224	I506S	9,b,s	rs193922522	G1298A	5,b
rs397508724	S158C	9,b,s	rs1800092	I506M	9,b,s	rs121909042	N1303H	9,e,f
rs397508727	L159S	8,b	rs74571530	F508C	7,b	rs121909042	N1303Y	9,e,f
rs397508729	Y161D	9,b,s	rs758745885	D513Y	4,e	rs397508636	N1303I	9,e,f
rs397508730	Y161S	9,b,s	rs368516826	C524R	8,b	rs80034486	N1303K	9,e,f
rs397508736	L165S	8,b	rs1387755887	G545V	9,b,s	rs201503139	P1306S	7,e
rs80282562	G178R	7,e	rs1469024267	L548P	9,b,s	rs397508646	D1312G	5,e
rs397508748	G178E	7,e	rs121908757	S519R	1,e	rs397508653	L1324P	7,b
rs397508751	L183I	9,b,s	rs121908755	S519I	1,e	rs755917129	I1267M	8,b
rs766640075	L188P	8,b	rs121909005	S519R	1,e	rs145545286	L1335F	7,b
rs397508756	D192N	9,e,f	rs75527207	G551D	9,e,f	rs397508660	L1339F	6,e
rs397508758	D192G	9,e,f	rs397508255	R555G	9,e,f	rs544710550	L1339P	6,e
rs755405930	E193G	3,e	rs75549581	A559S	9,b,s	rs747324955	G1343S	8,e,f
rs376008630	G194R	5,e	rs397508259	A559E	9,b,s	rs773458471	G1343V	8,e,f
rs397508765	H199Q	9,b,s	rs397508260	R560G	9,e,f	rs1313341594	L1346Q	7,b
rs1457675231	F200S	4b	rs121909006	Y563N	8,b	rs201686600	G1349S	9,e,f
rs121908803	P205S	9,b,s	rs397508276	Y569D	6,b	rs113857788	Q1352H	9,e,f
rs397508769	P205R	9,b,s	rs397508277	Y569C	6,b	rs1252048837	L1356S	8,b
rs121908752	L206W	6,b	rs397508282	D572N	9,e,f	rs748223886	R1358T	9,e,f
rs1227994401	Q207H	8,e,f	rs748393295	D572E	9,e,f	rs397508670	A1364V	6,b
rs759719664	L180F	6,b	rs121908758	P574H	8,e,f	rs770345073	I1366F	8,b
rs397508776	W216C	5,b	rs1800100	R668C	9,e,f	rs200955612	I1366N	8,b
rs770891254	G226E	7,b	rs186089140	S737F	9,e,f	rs761271867	I1366M	8,b
rs397508785	Q237H	9,e,f	rs397508363	R766M	9,e,f	rs767002769	L1369F	8,b
rs397508789	G241W	6,e	rs1386366130	Q767H	9,e,f	rs760336091	D1370H	9,e,f

Our analysis identified 30 nsSNPs in the CFTR gene as highly deleterious, based on consistent predictions across 15 computational algorithms that were subsequently prioritized for molecular modeling and structural studies to evaluate their potential impact on CFTR protein dynamics.

Modeling and structure validation

The 3D structure of CFTR was generated using SWISS-MODEL with Q2IBA1.1.A (CFTR_CHLAE) as the template (Figure 4A). The selected template showed 98.31% sequence identity with the query sequence and yielded a GMQE score of 0.76, indicating a reliable monomeric model. The refined structure, processed through ModRefiner, was validated using the SAVES server suite. ProCheck analysis demonstrated 88.10% of residues in the core regions, with an additional 8.10% in allowed regions, giving 96.2% of residues in favorable conformations overall. ERRAT analysis reported a quality factor of 97.524, while Verify3D confirmed that 52.39% of residues had an acceptable 3D–1D score.

The model achieved a QMEAN4 score of –3.29 (Figure 4B), placing it within the range expected for high-quality structures of comparable size. The red star in the QMEAN plot denoted the global quality estimate, positioned within the favorable region, while the red-shaded area represented the most reliable quality zone. Moreover, TM-align analysis revealed that I105N (Figure 4C), K273Q (Figure 4D) and G1249R (Figure 4E) exhibited the highest RMSD values (0.93, 0.98, and 0.93 Å, respectively) and were selected for further molecular docking to evaluate potential structural alterations (Supplementary Table S4).

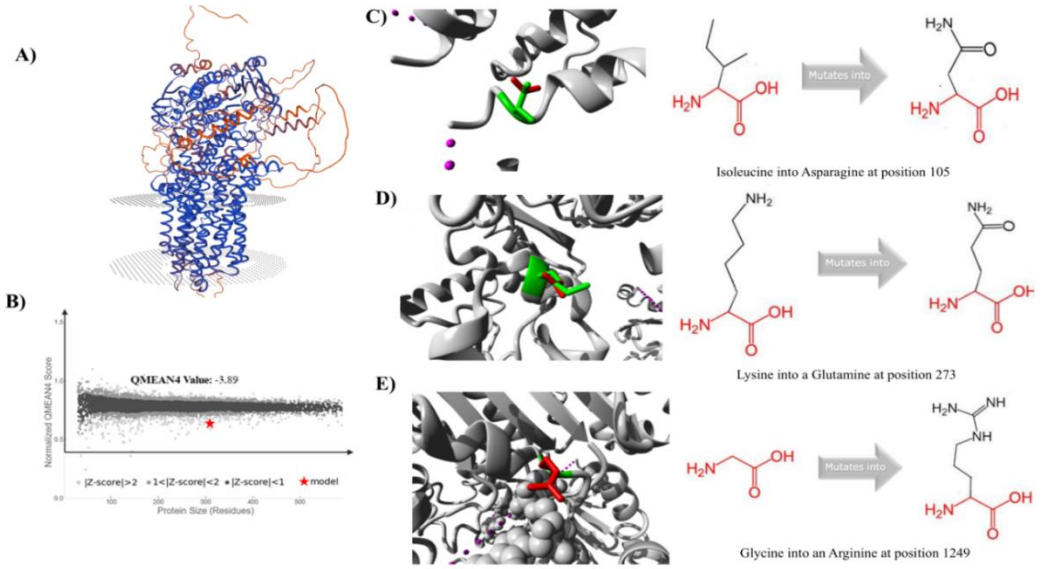

Fig. 4. Structural modeling and mutational analysis of the CFTR protein. **A)** Homology-modeled structure of the CFTR protein. **B)** QMEAN validation plot. **C)** Structural representation of the I105N mutation. **D)** Structural representation of the K273Q mutation. **E)** Structural representation of the G1249R mutation.

Table (4) summarizes the amino acid substitutions in the CFTR protein, their structural location, size differences, physicochemical changes, and the predicted impact on protein stability and function as assessed using the HOPE server. The stereochemical quality of the modeled CFTR structure was assessed using 2D and 3D Ramachandran plots across (a) general residues (Ala and the remaining 15 amino acids), (b) Gly, (c) Val/Ile, (d) pre-Pro, (e) trans-Pro, and (f) cis-Pro. In the 2D plots, torsion angles in favored, allowed, and disallowed regions were represented by cyan, blue, and red markers, respectively. Glycine residues were denoted by triangles, while all other residues were shown as dots. The 3D plots further illustrated the distribution of torsion angles by vertical bars, providing a quantitative overview of conformational preferences (Figure 5).

Table 4. Structural and Functional Consequences of CFTR Missense Variants Predicted by HOPE Analysis

rsID	A.A Change	Mutant Size	Effect on Protein	Variant Location	Amino Acid Properties
rs397508602	G1249R	Larger than wild-type	Disrupts ATP binding, destabilizes domain folding, and interferes with inter-domain communication	ATP-binding site	WT Gly: small, neutral, flexible; Mutant Arg: large, positively charged, less hydrophobic
rs1296578005	K273Q	Smaller than wild-type	Loss of H-bond with Ala959; disrupts salt bridges with Glu278 & Glu1172; destabilizes folding & interactions	Transmembrane domain	WT Lys: large, positively charged, hydrophilic; Mutant Gln: smaller, neutral, polar
rs397508509	I105N	Larger than wild-type	Introduces polar residue into hydrophobic core; disrupts packing; may abolish local folding & domain interactions	Transmembrane domain	WT Ile: small, hydrophobic, buried; Mutant Asn: larger, polar, less hydrophobic

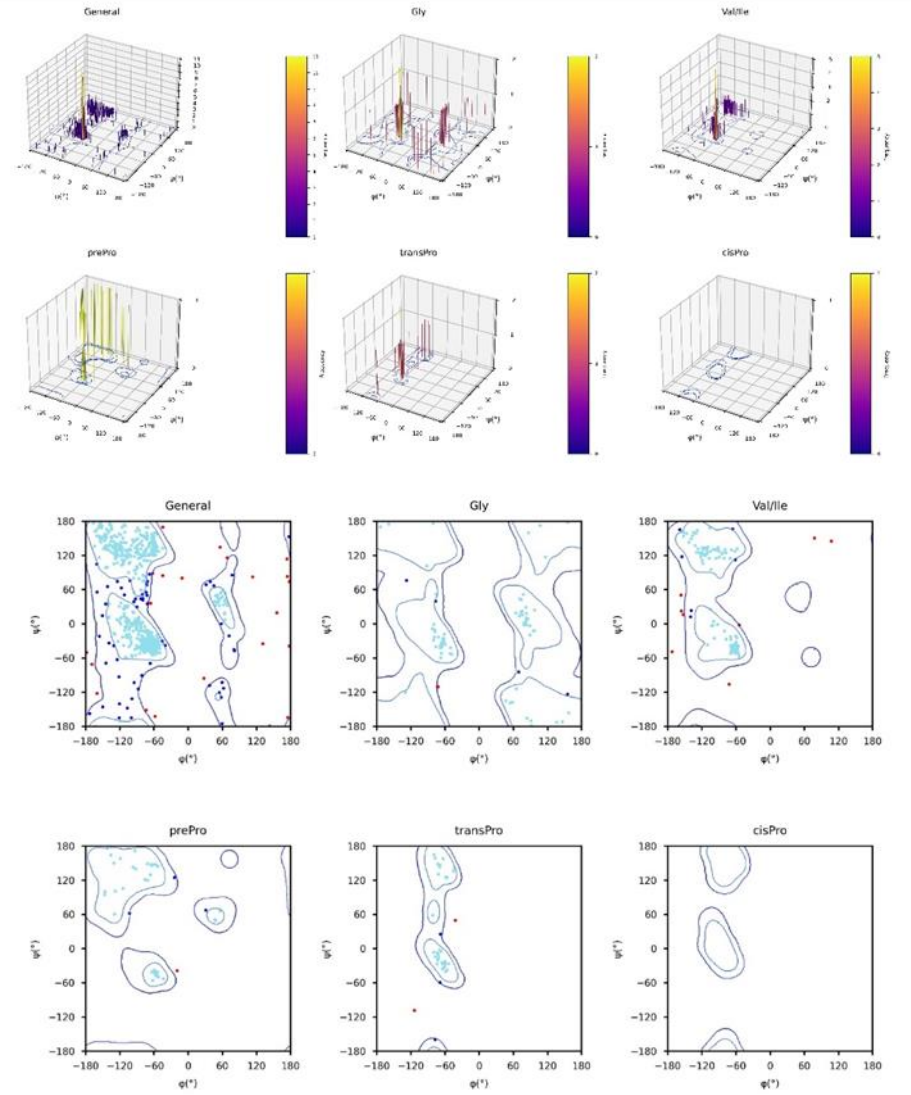

Fig. 5. 2D and 3D Ramachandran plots validating the stereochemical quality of the modeled CFTR structure.

Computational Docking of Wild-Type and Mutant CFTR Proteins

The molecular docking analysis demonstrated that all 25 ligands exhibited binding free energies lower than –4 kcal/mol when docked against the CFTR wild-type protein and I105N, K273Q, and G1249R variants. As shown in **Table 5**, the ligands with the most significant docking scores with Wild and mutant included Apoptozole, chromophore, Congo red, cpd β, cAMP, NAD, Nelfinavir, and melanin. The overall binding patterns were consistent with the known or predicted biological activities of these compounds. Moreover, chromophore (–9.1 kcal/mol with wild-type, –8.7 kcal/mol with K273Q, and –8.5 kcal/mol with G1249R) and apoptozole (–9.0, –8.5, –8.4 kcal/mol, respectively) showed the highest docking score, suggesting a potential to stabilize CFTR structures. Congo Red also demonstrated a high score across all variants, with scores ranging from –8.3 to –8.6 kcal/mol.

Table 5. PyRx-based molecular docking of ligands with CFTR wild-type and mutant variants.

Ligands	CFTR Wild	I105N	K273Q	G1249R	Ligands	CFTR Wild	I105N	K273Q	G1249R
Amprenavir	-6.9	-5.8	-6.2	-6.8	Memantine	-5.5	-5.5	-6	-4.9
Apoptozole	-9	-7.9	-8.5	-8.4	NAD	-6.9	-7.2	-8	-7.9
Biotin	-5.6	-5.9	-5.1	-5.1	Nelfinavir	-6.9	-7.1	-7.7	-7.8
cAMP	-7.3	-8	-7	-6.6	Phenothiazine	-6.3	-6	-6.4	-6.3
Chlorpromazine	-5.9	-5.3	-5.7	-5.3	3h-Indole-5,6 Diol	-5.3	-4.7	-6	-5.3
Chlortetracycline	-6.1	-6.3	-6.9	-7.1	3 ID	-6.4	-5	-5.9	-4.9
Chromophore	-9.1	-7.5	-8.7	-8.5	Alpha D-Fucopyranose	-5	-5.3	-4.9	-4.6
Congo Red	-8.6	-8.4	-8.3	-8.5	GLC	-5.5	-5.5	-4.9	-4.5
Cpd B	-7.9	-7.9	-7.5	-7.8	M2P	-6.2	-4.6	-4.7	-4.3
Florbetaben	-6.2	-5.7	-6	-5.4	TVY	-6.6	-6.3	-6	-5.5
GAG	-4.2	-4.6	-4.2	-3.9	Z8T	-5.3	-5.6	-4.6	-4.8
Hyaluronic Acid	-6.1	-6.5	-6.2	-6.1	Z9N	-4.2	-5.3	-4.3	-4.1
Melanin	-7.3	6.6	-7.8	-8.7					

Additionally, docking analysis revealed that antiviral agents like amprenavir and nelfinavir (–6.2 to –7.8 kcal/mol) and small molecules such as cAMP (–7.0 to –8.0 kcal/mol) interact strongly with CFTR, consistent with their roles in protein folding and CFTR activation. Phenothiazine, chlorpromazine, and natural metabolites, including NAD, biotin, hyaluronic acid, and melanin, showed moderate to strong affinities (–5.1 to –8.7 kcal/mol), suggesting potential effects on CFTR gating, stability, and cellular function. Table S5 details interacting residues, while 2D interaction patterns (Figure 6) highlight hydrogen bonds and hydrophobic contacts across wild-type and mutant CFTR, supporting opportunities for drug repurposing and novel CFTR modulators. Apoptozole interacted strongly with wild-type CFTR through multiple hydrogen bonds involving GLN376, LEU375, GLU379, GLN378, LYS381, LYS166, TRP57, and GLU54, with hydrophobic associations contributed by LYS377, LEU61, PRO67, LEU159, and LYS162. In the G1249R mutant, apoptozole established hydrogen bonds with LEU1279, ARG1259, THR1278, LEU1187, ALA959, SER955, THR1176, GLU279, and GLN1280, and hydrophobic contacts with ILE1277, GLN1186, GLY1185, GLN958, PRO1175, PRO960, GLU278, and LEU957. In I105N, it formed hydrogen bonds with GLU402, SER431, GLY437, ASP173, PHE430, SER176, and LEU428, while hydrophobic interactions involved ARG170, LEU436, PHE405, SER431, TRP401, and LYS174. For K273Q, apoptozole bound via hydrogen bonds with GLN1280, ASP1275, THR1278, GLU278, GLN158, ALA959, THR1176, PRO960, ASN1262, LEU1261, LYS1177, ARG1259, and MET96, in addition to hydrophobic associations with TRP1274, ILE1277, and PRO1175 (Table S5).

Chromophore exhibited extensive hydrogen bonding with residues such as ASN1262, SER962, LEU1260, ASP1275, ILE1277, TRP1274, LYS1177, THR1278, GLU1280, and GLN258 in wild-type CFTR, with hydrophobic contacts mainly at LEU1279 and ARG1259. In the G1249R mutant, chromophore formed hydrogen bonds with GLU278, ARG1283, LEU1261, MET961, ARG1259, LEU1260, PRO960, TRP1274, LYS1177, ILE1277, THR1278, ASN1184, PRO1175, ASP1275, ALA595, THR1176, and GLN958, and hydrophobic interactions at LYS273 and LEU1279. In I105N, it bound through hydrogen bonds with ARG1283, GLU1221, ASN1262, THR1220, SER962, LEU1261, TRP1274, THR1278, ILE1277, ALA959, PRO1175, THR1176, LYS273, GLN958, and PRO960, while hydrophobic interactions involved ARG1259 and LEU1279. For K273Q, chromophore mainly bound through hydrogen bonds with PHE430, GLN179, ASP373, LYS370, LEU183, LYS377, PHE374, VAL1171, ARG170, and LEU428, and showed hydrophobic contacts with LYS174, ILE175, and PHE429 (Table S5). Congo red in the wild type formed

hydrogen bonds with ARG1259, LEU1260, LEU1279, TRP1274, SER1276, ASN1184, THR1278, ILE1177, LYS1177, SER962, GLU1221, ASN1262, LEU1261, MET961, and GLN1186, and hydrophobic associations with LEU1187 and PRO96. In the G1249R mutant, hydrogen bonds were observed with VAL171, GLN179, SER182, ASN186, ASN187, ILE371, PHE374, ARG170, LYS370, and GLN378, while hydrophobic contacts involved LYS174, LYS377, LEU183, and ILE175. In I105N, Congo red interacted through hydrogen bonds with GLN958, HIS954, ASN1184, LYS1183, SER1276, ASP1275, ILE1277, GLN1280, LYS273, GLU282, and GLU279, with hydrophobic associations at SER1188, LYS1177, GLU278, LEU957, and THR1278. In K273Q, hydrogen bonds were seen with SER1178, LYS1180, GLY1185, PRO1175, ARG1259, LYS1177, GLN258, GLN273, ALA259, ARG1283, and LEU1260, with hydrophobic interactions at PRO960, THR1176, LEU1279, ASN1184, and LYS1183 (Table S5).

Additionally, Cpd β bound wild-type CFTR through hydrogen bonds with SER1188, THR1278, THR1263, ASN1184, SER1276, ILE1222, TRP1224, LEU1260, SER962, and LEU1961, while hydrophobic contacts involved LEU1229, ARG1259, MET961, PRO960, ASN1262, and LEU1229. In I105N, hydrogen bonding was observed with CYS276, HIS954, GLU282, GLN958, LYS273, GLN1280, GLN1309, and TYR1307, alongside hydrophobic contacts with GLU279, LEU957, and GLU278 (Table S5). Moreover, cAMP in the wild type showed hydrogen bonding with GLN378, LYS181, TYR380, SER168, GLU474, ARG170, LEU475, TRP401, SER478, and PRO477, and hydrophobic interactions with GLU476 and GLU403. In I105N, cAMP formed hydrogen bonds with ASN1262, MET961, ALA959, ARG1283, LYS273, GLN958, PRO1175, PRO960, LEU1260, LEU1261, THR1263, and ASN126, and a hydrophobic contact with ARG1259 (Table S5).

Furthermore, Melanin bound wild-type CFTR through hydrogen bonds with TYR1073, GLU504, PRO499, THR1053, HIS1054, THR1057, and PHE1074, together with hydrophobic interactions involving LEU1077. In the G1249R mutant, melanin interacted through hydrogen bonds with SER422, ASN423, GLU424, PHE409, LYS411, ALA412, LYS413, GLU410, and GLN414, and hydrophobic associations with THR421 and ALA412. In the K273Q mutant, hydrogen bonding occurred with ILE175, PHE374, LYS377, LEU183, GLN179, and SER182, and hydrophobic contacts with ASP373 and LYS370. Finally, NAD interacted with wild-type CFTR through hydrogen bonds with GLN958, LEU1260, MET961, ARG1259, PRO960, LEU1261, THR1263, ASN1262, SER962, THR1220, GLU1221, LYS1174, THR1776, GLU278, ALA959, and LEU957, with hydrophobic associations at ARG1283 and LYS273. In the G1249R mutant, similar interactions were observed with key residues, while in I105N, NAD formed hydrogen bonds with ARG1283, LEU1260, LEU1261, LEU1279, ASN1262, TRP1274, LYS1177, GLN1186, ASN1184, ALA959, GLN958, GLY1185, SER1188, SER1276, THR1278, MET961, PRO960, and PRO1175, along with hydrophobic contacts with ILE1277 and ARG1259 (Table S5).

Such ligands showed strong docking scores with both wild-type and mutant CFTR proteins, suggesting their potential as scaffolds for CFTR modulators. Structure-based refinement, molecular dynamics, and functional assays are essential to validate these candidates and optimize their selectivity, stability, and pharmacokinetics. Promising compounds should progress to cellular and in vivo studies, with delivery strategies such as oral or inhaled formulations enhancing therapeutic relevance. Repurposed agents like nelfinavir may accelerate approval, while novel scaffolds will require extensive preclinical testing. An integrated pipeline combining computational, experimental, and regulatory approaches offers a path toward effective CFTR-targeted therapies.

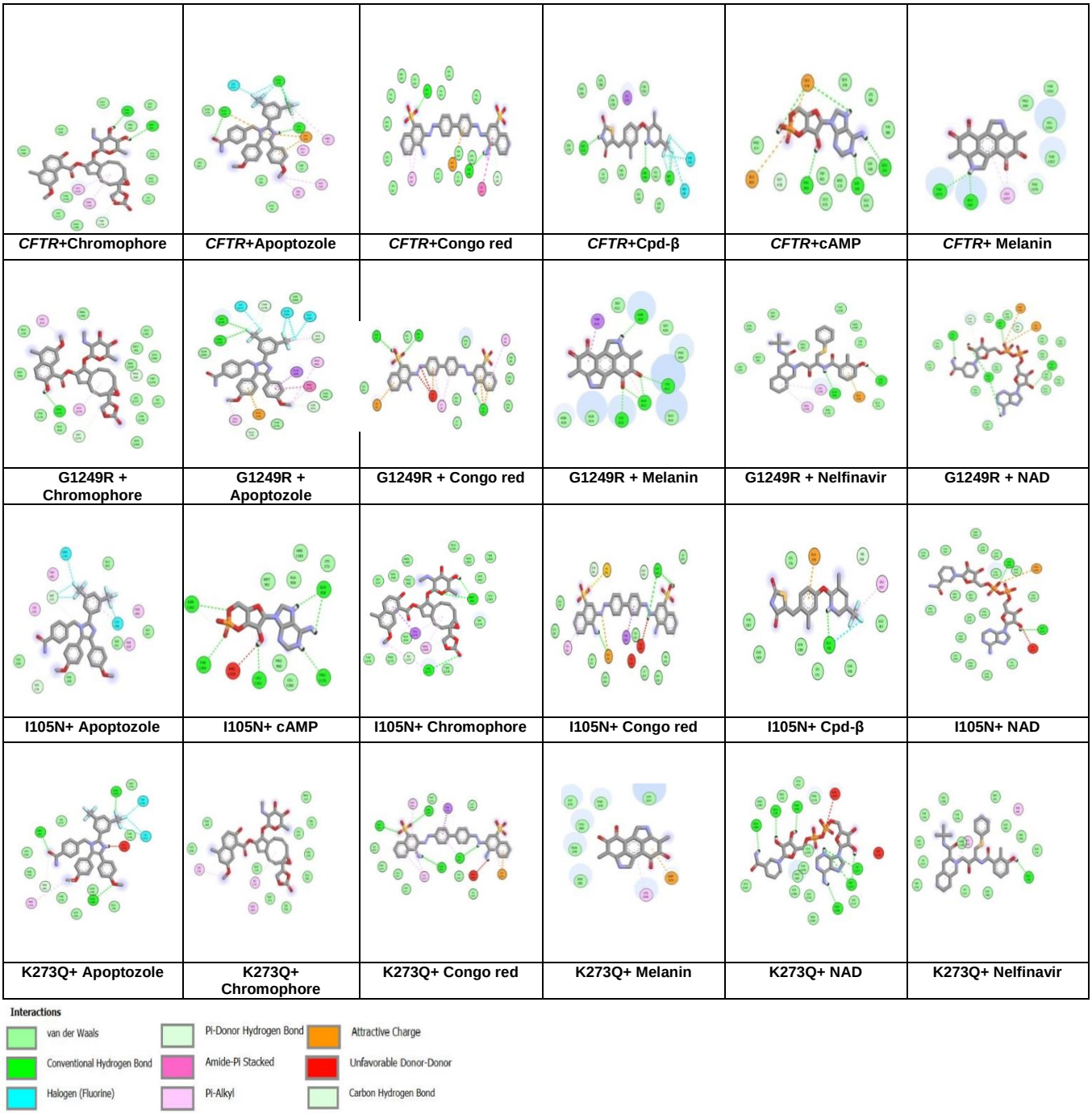

Fig. 6. Visualization of ligand interactions with native CFTR and its variants (I105N, K273Q, and G1249R) using Discovery Studio Visualizer.

DISCUSSION

Cystic fibrosis (CF) is a common inherited multisystem disorder caused by CFTR mutations, affecting the respiratory, gastrointestinal, and reproductive systems (Fonseca *et al.*, 2020). First linked to leukotriene production in 1981, CFTR was mapped to chromosome 7q31.2 in 1989 and characterized with 24 exons. Over 4,000 mutations have been reported, with F508del (~70% of alleles) being the most prevalent, alongside G542X, N1303K,

G551D, and W1282X (Donos *et al.*, 2025; Ideozu *et al.*, 2024a; Ramananda *et al.*, 2024). Amino acid substitutions account for over 40% of variants, and SNPs are the main source of genetic diversity, cataloged in CFTR1 databases. Computational approaches help predict structural and functional impacts of CFTR mutations, allowing identification of high-risk nsSNPs for experimental validation and drug development. This study employed an integrated computational strategy to evaluate CFTR nsSNPs and identify potential therapeutic modulators (Michels *et al.*, 2019). Multiple tools were used to predict pathogenicity, disease association, stability, residue conservation, and post-translational modifications. Homology models of wild-type and mutant CFTR were built and validated with SWISS-MODEL, ModRefiner, SAVES, Ramplot, QMEAN, and TM-align, while HOPE analyzed physicochemical effects of substitutions. Molecular docking with PyRx (AutoDock Vina) using PubChem and literature-sourced ligands revealed altered interactions in mutant proteins. The findings highlight high-risk nsSNPs that destabilize CFTR, disrupt ligand binding, and provide targets for experimental validation and drug development (Ramzan and Noman, 2024; Rasheed *et al.*, 2025).

From an initial dataset of 282,490 SNPs, 10,618 were non-synonymous, indicating potential functional relevance. SIFT and PolyPhen consistently predicted 132 nsSNPs as deleterious, forming a high-confidence subset. Further analyses with SNAP2, PROVEAN, CADD, ConDEL, SNPs&GO, P-Mut, PhD-SNP, and Meta-SNP largely confirmed their pathogenicity, with few variants consistently neutral. Protein stability predictions using i-Mutant 3.0, MUPro, and i-Stable showed that 106 nsSNPs reduce CFTR stability. CONSURF analysis revealed 98 variants in highly conserved residues, 46 of which scored maximally, emphasizing functional importance. Post-translational modification predictions identified C524, S707, and S737 as potentially affecting CFTR activity. Thirty nsSNPs were prioritized for structural analysis based on consistent deleterious predictions across 15 algorithms. Available PDB structures are partial, often representing only wild-type CFTR, while disease-relevant mutations like I105N, K273Q, and G1249R are absent. Notably, PDB 6MSM depicts ATP-bound, phosphorylated CFTR, 5UAK shows NBD1 with regulatory elements, and 5W81 includes NBD1 with F508del, illustrating mutation-induced structural disruptions (d'ursi *et al.*, 2020; Zacarias *et al.*, 2023).

Homology modeling with SWISS-MODEL enabled generation of complete, mutation-specific CFTR structures with structural refinement and energy minimization. Using Q2IBA1.1.A (CFTR_CHLAE) as a template, the model achieved 98.31% sequence identity and a GMQE of 0.76. Refinement via ModRefiner and validation with SAVES showed 96.2% of residues in favorable conformations (ProCheck), an ERRAT score of 97.524, Verify3D acceptability of 52.39%, and a QMEAN4 of –3.29, confirming reliability. TM-align indicated that I105N, K273Q, and G1249R had the highest RMSD values (0.93–0.98 Å), reflecting notable conformational changes. HOPE analysis revealed substitutions affecting size, charge, and hydrophobicity, likely impacting stability and function. Ramachandran analysis in 2D and 3D confirmed most torsion angles in favored or allowed regions, with minimal residues in disallowed regions, validating stereochemical integrity.

Molecular docking predicts interactions between ligands and target proteins, providing insights into binding affinity, specificity, and potential biological activity. Docking against CFTR and its variants identified ligands with strong modulatory potential, including apoptozole, chromophore, Congo Red, cpd β, cAMP, NAD, Nelfinavir, and melanin. cAMP enhances CFTR activity via PKA-mediated phosphorylation, while phenothiazine and chlorpromazine influence channel gating and trafficking. Antiviral agents like amprenavir and nelfinavir may aid misfolded CFTR rescue by modulating protein folding and ER stress, and apoptozole, an Hsp70 inhibitor, may improve CFTR stabilization. Congo Red and chromophores likely act as chemical chaperones, stabilizing misfolded conformations. Natural metabolites such as NAD, biotin, hyaluronic acid, and melanin may support CFTR

stability through redox regulation, energy metabolism, and antioxidant effects. These findings highlight diverse ligands with potential for rescuing defective CFTR and guiding drug repurposing and novel modulator discovery for cystic fibrosis therapy (Della Sala *et al.*, 2021; Lobo *et al.*, 2016).

Our results showed that Chromophore (–9.1 kcal/mol) and apoptozole (–9.0 kcal/mol) had the highest binding affinities, suggesting strong potential to stabilize CFTR. Congo Red, amprenavir, and nelfinavir exhibited moderate binding (–6.2 to –7.8 kcal/mol), consistent with roles in protein folding and stress response modulation, while cAMP (–7.0 to –8.0 kcal/mol) reinforced its known PKA-mediated activation of CFTR. Natural cofactors, including NAD, biotin, hyaluronic acid, and melanin, displayed favorable binding (–5.1 to –8.7 kcal/mol) and maintained interactions across all variants (–8.3 to –8.6 kcal/mol), indicating potential contributions to CFTR stabilization through metabolic or antioxidant mechanisms. Detailed interaction analysis revealed extensive hydrogen bonds and hydrophobic contacts with key residues. For example, apoptozole engaged GLN376, LEU375, and LYS162 in the wild type, and LEU1279, ARG1259, and THR1278 in the G1249R mutant. Chromophore, Congo Red, cpd β, cAMP, NAD, and melanin similarly formed stable interactions within CFTR pockets, highlighting promising scaffolds for drug discovery and repurposing. Translating these findings to therapeutics will require electrophysiological assays, protein folding studies, molecular dynamics, and binding free energy analyses. ADMET profiles are generally favorable, though solubility, stability, and inhaled delivery may need optimization. Repurposed drugs like nelfinavir and amprenavir could advance rapidly, whereas novel scaffolds such as apoptozole or chromophore derivatives will require extensive preclinical evaluation (Kumar *et al.*, 2024). The identified binding sites align with Odolczyk's findings (Odolczyk *et al.*, 2013), highlighting two NBD1 pockets and residues F494, W496, K1060, and W1063 as critical for corrector activity. Confirmation via site-directed mutagenesis and validation with molecular dynamics and free energy calculations is necessary. While CFTR-targeted therapies like ivacaftor and VX-809 improve survival, longer lifespans introduce new risks, including cancer susceptibility, reflecting CFTR's broader roles in growth, differentiation, and regeneration. Computational predictions must therefore be integrated with mutational, biophysical, and clinical studies to refine therapies and guide genetic counseling (Allan *et al.*, 2022; Lester *et al.*, 2023).

CONCLUSION

This study applied an in-silico pipeline to assess deleterious CFTR nsSNPs and identify potential modulators through molecular docking. We found that 30 nsSNPs were predicted as highly deleterious, with I105N, K273Q, and G1249R showing major destabilizing effects on CFTR structure and function. Docking revealed strong ligand affinities, notably for apoptozole, chromophore, Congo Red, NAD, melanin, and cAMP, while repurposed drugs such as nelfinavir and amprenavir also showed promising interactions. These results highlight key pathogenic variants and suggest opportunities for drug repurposing and modulator development, providing a foundation for experimental validation and personalized therapies in cystic fibrosis.

CONFLICT OF INTEREST

The author declares this article content has no conflict of interest.

REFERENCES

AbdulAzeez, S., Borgio, J.F., 2016. In-silico computing of the most deleterious nsSNPs in HBA1 gene. PloS one, 11(1): e0147702.

Abuzaid, O., Idris, A.B., Yılmaz, S., Idris, E.B., Idris, L.B., Hassan, M.A., 2024. Prediction of the most deleterious non-synonymous SNPs in the human IL1B gene: evidence from bioinformatics

analyses. BMC Genom. Data., 25(1): 56.

Adeniji, S.E., Uba, S., Uzairu, A., 2020. In silico study for evaluating the binding mode and interaction of 1, 2, 4-triazole and its derivatives as potent inhibitors against Lipoate protein B (LipB). J. King Saud Univ. Sci., 32(1): 475-485.

Allan, K.M., Astore, M.A., Fawcett, L.K., Wong, S.L., Chen, P.C., Griffith, R., Jaffe, A., Kuyucak, S., Waters, S.A., 2022. S945L-CFTR molecular dynamics, functional characterization and tezacaftor/ivacaftor efficacy in vivo and in vitro in matched pediatric patient-derived cell models. Front. Pediatr., 10: 1062766.

Armon, A., Graur, D., Ben-Tal, N., 2001. ConSurf: an algorithmic tool for the identification of functional regions in proteins by surface mapping of phylogenetic information. J. Mol. Biol., 307(1): 447-463.

Bilal, I., Munir, H., Ramzan, K., Zulfiqar, I., Waheed, A., Haider, A.L.I., Ali, F., 2025a. Structural modeling and functional prediction of IFN-Y gene variants. Quantum J. Med. Health Sci., 4: 84-102.

Bilal, I., Ramzan, K., Ramzan, S., Zulfiqar, M., Tahir, U., Moazzam Qadri, A., Haider, I., 2025b. Homology Modeling and Structural Docking Analysis on a Human BDNF Gene by Using Computational Algorithms. J. Adv. Biol. Biotechnol., 28: 464-487.

Chandrasekaran, G., Hwang, E.C., Kang, T.W., Kwon, D.D., Park, K., Lee, J.-J., Lakshmanan, V.-K., 2017. Computational modeling of complete hoxb13 protein for predicting the functional effect of snps and the associated role in hereditary prostate cancer. Sci. Rep., 7(1): 1-18.

d'ursi, P., Pedemonte, N., Urbinati, C., Ford, R., Cichero, E., Uggeri, M., Orro, A., Fossa, P., 2020. Recent Strategic Advances in CFTR Drug Discovery: An Overview. Int. J. Mol. Sci., 21: 2407.

Deletang, K., Taulan-Cadars, M., 2022. Splicing mutations in the CFTR gene as therapeutic targets. Gene Ther., 29(7-8): 399-406.

Della Sala, A., Prono, G., Hirsch, E., Ghigo, A., 2021. Role of Protein Kinase A-Mediated Phosphorylation in CFTR Channel Activity Regulation. Front. Physiol., 12 - 2021.

Donos, M.A., Butnariu, L.I., Anton Păduraru, D.T., Murgu, A.M., Rusu, C., Pânzaru, M.C., Popescu, R., Țarcă, E., Cojocaru, E., Ghiga, G., Trandafir, L.M., 2025. Genetic Heterogeneity Correlated with Phenotypic Variability in 48 Patients with Cystic Fibrosis. J. Clin. Med., 14(15).

Doss, C.G.P., Rajasekaran, R., Sudandiradoss, C., Ramanathan, K., Purohit, R., Sethumadhavan, R., 2008. A novel computational and structural analysis of nsSNPs in CFTR gene. Genom. Med., 2(1): 23-32.

Fonseca, C., Bicker, J., Alves, G., Falcão, A., Fortuna, A., 2020. Cystic fibrosis: Physiopathology and the latest pharmacological treatments. Pharmacol. Res., 162: 105267.

Hasan, M.M., Khatun, M.S., 2018. Prediction of protein post-translational modification sites: an overview. Ann. Proteom. Bioinform., 2: 049-57.

Hasnain, M.J.U., Shoaib, M., Qadri, S., Afzal, B., Anwar, T., Abbas, S.H., Sarwar, A., Talha Malik, H.M., Tariq Pervez, M., 2020. Computational analysis of functional single nucleotide polymorphisms associated with SLC26A4 gene. Plos One, 15(1): e0225368.

Heidarinia, H., Tajbakhsh, E., Bahrami, Y., Rostamian, M., 2025. Design a multi-epitope vaccine candidate against Acinetobacter baumannii using advanced computational methods. AMB Express., 15(1): 103.

Ideozu, J., Liu, M., Riley-Gillis, B., Paladugu, R., Rahimov, F., Krishnan, P., Tripathi, R., Dorr, P., Levy, H., Singh, A., Waring, J., Vasanthakumar, A., 2024a. Diversity of CFTR variants across ancestries characterized using 454,727 UK biobank whole exome sequences. Genom. Med., 16.

Ideozu, J.E., Liu, M., Riley-Gillis, B.M., Paladugu, S.R., Rahimov, F., Krishnan, P., Tripathi, R., Dorr, P., Levy, H., Singh, A., Waring, J.F., Vasanthakumar, A., 2024b. Diversity of CFTR variants across ancestries characterized using 454,727 UK biobank whole exome sequences. Genom. Med., 16(1): 43.

Kamal, M.M., Shantanu, K.F.H., Teeya, S.T., Rahman, M.M., Hasan, A., Chivers, D.P., Wani, T.A., Alshammari, A.H., Rachamalla, M., da Silva Junior, F.C., Hossen, M.M., 2025. Investigating the functional and structural effect of non-synonymous single nucleotide polymorphisms in the cytotoxic T-lymphocyte antigen-4 gene: An in-silico study. PLoS One, 20(1): e0316465.

Kumar, M., Rathore, R., 2025. RamPlot : a webserver to draw 2D, 3D and assorted Ramachandran (φ, ψ) maps. J. Appl. Crystallogr., 58.

Kumar, V., Barwal, A., Sharma, N., Mir, D.S., Kumar, P., Kumar, V., 2024. Therapeutic proteins: developments, progress, challenges, and future perspectives. 3 Biotech, 14(4): 112.

Kumari, A., Mittal, I., Kaushik, A., Jaitly, A., Nain, N., Toor, D.S., Pal, T., Saini, S., Thakur, C.J., 2025. A comprehensive computational study of non-synonymous SNPs (nsSNPs) of NTRK1 Gene using conservation, stability, docking, and simulation approaches. In Silico Res. Biomed., 1: 100053.

Lester, A., Sandman, M., Herring, C., Girard, C., Dixon, B., Ramsdell, H., Reber, C., Poulos, J., Mitchell, A., Spinney, A., Henager, M.E., Evans, C.N., Turlington, M., Johnson, Q.R., 2023. Computational Exploration of Potential CFTR Binding Sites for Type I Corrector Drugs. Biochem., 62(16): 2503-2515.

Lobo, M., Amaral, M., Zaccolo, M., Farinha, C., 2016. EPAC1 activation by cAMP stabilizes CFTR at the membrane by promoting its interaction with NHERF1. J. Cell Sci., 129: 185629.

López-Ferrando, V., Gazzo, A., De La Cruz, X., Orozco, M., Gelpí, J.L., 2017. PMut: a web-based tool for the annotation of pathological variants on proteins, 2017 update. Nucleic Acids Res., 45(W1): W222-W228.

Magesh, R., Doss, C.G.P., 2014. Computational pipeline to identify and characterize functional mutations in ornithine transcarbamylase deficiency. 3 Biotech, 4(6): 621-634.

Mathew, A., Dirawi, M., Abou Tayoun, A., Popatia, R., 2021. A Rare Cystic Fibrosis Transmembrane Conductance Regulator (CFTR) Mutation Associated With Typical Cystic Fibrosis in an Arab Child. Cureus, 13(2): e13526.

Michels, M., Matte, U., Fraga, L.R., Mancuso, A.C.B., Ligabue-Braun, R., Berneira, E.F.R., Siebert, M., Sanseverino, M.T.V., 2019. Determining the pathogenicity of CFTR missense variants: Multiple comparisons of in silico predictors and variant annotation databases. Genet. Mol. Biol., 42(3): 560-570.

Odolczyk, N., Fritsch, J., Norez, C., Servel, N., da Cunha, M.F., Bitam, S., Kupniewska, A., Wiszniewski, L., Colas, J., Tarnowski, K., Tondelier, D., Roldan, A., Saussereau, E.L., Melin-Heschel, P., Wieczorek, G., Lukacs, G.L., Dadlez, M., Faure, G., Herrmann, H., Ollero, M., Becq, F., Zielenkiewicz, P., Edelman, A., 2013. Discovery of novel potent ΔF508-CFTR correctors that target the nucleotide binding domain. EMBO Mol. Med., 5(10): 1484-501.

Parisi, G.F., Mòllica, F., Giallongo, A., Papale, M., Manti, S., Leonardi, S., 2022. Cystic fibrosis transmembrane conductance regulator (CFTR): beyond cystic fibrosis. Egypt. J. Med. Hum. Genet., 23(1): 94.

Purushothaman, A.K., Nelson, E.J.R., 2023. Role of innate immunity and systemic inflammation in cystic fibrosis disease progression. Heliyon, 9(7): e17553.

Rafique, H., Safdar, A., Ghani, M.U., Akbar, A., Awan, F.I., Naeem, Z., Amar, A., Awan, M.F., Wajahat Ullah, S., Shaikh, R.S., 2024. Exploring the diversity of CFTR gene mutations in cystic fibrosis individuals of South Asia. J. Asthma., 61(6): 511-519.

Ramananda, Y., Naren, A.P., Arora, K., 2024. Functional Consequences of CFTR Interactions in Cystic Fibrosis. Int. J. Mol. Sci., 25(6): 3384.

Ramzan, K., Noman, A., 2024. Structural Analysis And Protein-Ligand Docking Approach Of BrainAssociated APOE, SNCA, And PRKN Genes. Int. J. Pharm. Sci., 2: 393-410.

Rasheed, A., Safdar, M., Umar, A., Khan, M.S., Ramzan, S., Ramzan, K., Sabri, S., Shaffique, S., Tahir, M.Z., 2025. Comparative bioinformatics analysis and functional characteristics of natriuretic peptide B (NPPB) gene in humans. In Silico Research in Biomedicine, 1: 100074.

Sharma, A., Mahur, P., Singh, A.K., Muthukumaran, J., Jain, M., 2024. Insights into the structural and functional analysis of impact of the missense mutations on α-synuclein: an in silico study. Egypt. J. Med. Hum. Genet., 25(1): 60.

Subbiah, H.V., Babu, P.R., Subbiah, U., 2020. In silico analysis of non-synonymous single nucleotide polymorphisms of human DEFB1 gene. Egypt. J. Med. Hum. Genet., 21(1): 1-9.

Tariq, H., Asif, M., Saleem, M., Ramzan, K., Zulfiqar, M., Amir, A., Asif, A.R., 2024a. Evaluation of Detrimental Missense SNPs of Human CXCL6 Gene by Combining Algorithms, Homology Modeling, and Molecular Docking. Inv. Biol., 4(4): 92-106.

Tariq, H., Aslam, T., Saleem, M., Ramzan, K., 2024b. Bioinformatic Analysis of Human TLR4 Coding Variations Associated with Ocular Infection: A Structural Prediction and Molecular Docking Studies. Int. J. Pharm. Sci., 2: 930-954.

Waheed, S., Ramzan, K., Ahmad, S., Khan, M.S., Wajid, M., Ullah, H., Umar, A., Iqbal, R., Ullah, R., Bari, A., 2024. Identification and In-Silico study of non-synonymous functional SNPs in the human SCN9A gene. PloS One, 19(2): e0297367.

Wang, D., Liu, D., Yuchi, J., He, F., Jiang, Y., Cai, S., Li, J., Xu, D., 2020. MusiteDeep: a deep-learning based webserver for protein post-translational modification site prediction and visualization. Nucleic Acids Res., 48(W1): W140-W146.

Zacarias, S., Batista, M., Ramalho, S., Victor, B., Farinha, C., 2023. Rescue of Rare CFTR Trafficking Mutants Highlights a Structural Location-Dependent Pattern for Correction. Int. J. Mol. Sci., 24: 3211.

Zhang, B., Zhang, Y., Zhang, Y., Liu, X., Zhang, R., Wang, Z., Pan, F., Xu, N., Shao, L., 2025. Identified five variants in CFTR gene that alter RNA splicing by minigene assay. Front. Genet., 16: 1543623.

Zhu, J., 2024. The bioinformatic analysis of CFTR in essential hypertension. Theor.Nat. Sci., 29: 92-100.